Sección Especial: IX Reunión Nacional de Óptica

Optic disc segmentation in retinal images

Segmentación del disco óptico en imágenes de la retina

Andrés G. Marrugo[(*,S)] and María S. Millán[(S)]

Grup d'Òptica Aplicada i Processament d'Imatge, Departament d'Òptica i Optometria, Univesitat Politècnica de Catalunya, Terrassa.

[(*)] Email: andres.marrugo@upc.edu S: miembro de SEDOPTICA / SEDOPTICA member

Recibido / Received: 30/11/2009. Versión revisada / revised versión: 29/03/2010. Aceptado / Accepted: 30/03/2010

ABSTRACT:

Retinal images are widely used for diagnostic purposes by ophthalmologists. Therefore, these images are suitable for digital image analysis for their visual enhancement and pathological risk or damage detection. Here, we discuss two different approaches towards optic disc segmentation. We review and analyze a prior work based on a pixel-wise contour extraction for optic nerve head segmentation along with the effects of processing retinal images under lossy compression. This analysis revealed the need for a more general and robust approach. Finally, we introduce a different strategy for optic disc segmentation based on the use of active contours and color mathematical morphology.

Key words: Retinal Image, Optic Disc, Eye Fundus, Medical Imaging, Segmentation, Image Analysis.

RESUMEN:

Las imágenes de la retina son ampliamente utilizadas para el diagnóstico clínico por oftalmólogos. Por tanto, estas imágenes pueden ser procesadas digitalmente, tanto para su realce como para detección de riesgo patológico. En este trabajo se presentan dos vías para la segmentación del disco óptico. Partimos de un trabajo previo sobre la extracción del contorno del disco óptico, y analizamos los efectos producidos por un procesado de la imagen retiniana bajo compresión con pérdidas. De este análisis resulta evidente la necesidad de un algoritmo con un enfoque más general y robusto. Por último, presentamos una estrategia diferente para la segmentación del disco óptico basado en el uso de contornos activos y morfología matemática en el espacio de color.

Palabras clave: Imagen Retiniana, Fondo de Ojo, Disco Óptico, Imagen Médica, Segmentación, Análisis de Imagen.

REFERENCES AND LINKS

[1] N. Patton, T. M. Aslam, T. MacGillivray, I. J. Deary, B. Dhillon, R. H. Eikelboom, K. Yogesana, I. J. Constable, "Retinal image analysis: Concepts, applications and potential", *Prog. Retin. Eye Res.* **25**, 99–127 (2006).

[2] N. Harizman, C. Oliveira, A. Chiang, C. Tello, M. Marmor, R. Ritch, J.M. Liebmann, "The ISNT rule and differentiation of normal from glaucomatous eyes", *Arch. Ophthalmol*. **124**, 1579-1583 (2006).

[3] T. Walter, J. C. Klein, P. Massinm, A. Erginay, "A contribution of image processing to the diagnosis of diabetic retinopathy – detection of exudates in color fundus images of the human retina", *IEEE T. Med. Imaging* **21**, 1236-1243 (2002).

[4] H. Li, O. Chutatape, "Boundary detection of optic disk by a modified ASM method", *Pattern Recogn.* **36**, 2093-2104 (2003).

[5] E. Valencia, M. S. Millán, R. Kotynski, "Cup-to-disc ratio of the optic disc by image analysis to assist diagnosis of glaucoma risk and evolution," in *Information Optics: 5th International Workshop*, G. Cristóbal, B. Javidi, S.Vallmitjana Edts., American Institute of Physics, CP860, 290-299 (2006).

[6] E. Valencia, M. S. Millán, "Color image sharpening and application to eye fundus image analysis," RIAO/OPTILAS 2007, edited by N.U. Wetter, J. Freijlich, American Institute of Physics CP992, 39-44 (2008).

[7] A. G. Marrugo, M. S. Millán, "Efectos de compresión en imágenes de la retina para la evaluación del riesgo glaucomatoso", IX Reunión Nacional de Óptica, Sociedad Española de Óptica, Orense, 140 (2009).

[8] F. Mendels, C. Heneghan, P.D. Harper, R.B. Reilly, J. P. Thiran, "Extraction of the optic disk boundary in digital fundus images", Proc. First Joint BMES/EMBS Conference, **2**, 1139 (1999).

[9] A. Osareh, M. Mirmehdi, B. Thomas, R. Markham, "Comparison of colour spaces for optic disc localisation in retinal images", 16th Int. Conf. on Pattern Recognition **1**, 743–746 (2002).

[10] H. Zhou, G. Schaefer, T. Liu, F. Lin, "Segmentation of optic disc in retinal images using an improved gradient vector flow algorithm", *Multimed. Tools Appl.* (2010) Online: doi 10.1007/s11042-009-0443-0

[11] M.S. Millán, E. Valencia, "Color image sharpening inspired by human vision models", *Appl. Opt.* **45**, 7684–7697 (2006).

[12] G. M. Johnson, M.D. Fairchild, "A top down description of the S-CIELAB and CIEDE2000", *Color Res. Appl*. **28**, 425–435 (2003).

[13] X. Zhang, B. A. Wandell, "A spatial extension to CIELAB for digital color image reproduction", *Soc. Fo Info. Disp. Symp. Tech. Digest* **27**, 731–734 (1996).

[14] T. F. Chan, L. A. Vese, "Active contours without edges", *IEEE T. Image Process.* **10**, 266–277 (2001).

[15] J. Conrath, "Evaluation of the effect of JPEG and JPEG2000 image compression on the detection of diabetic retinopathy", *Eye* **21**, 487-493 (2006).

[16] R. J. Winder, P. J. Morrow, I. N. McRitchie, J. R. Bailie, P. M. Hart, "Algorithms for digital image processing in diabetic retinopathy", *Comput. Med. Imag. Grap.* **33**, 608-622 (2009).

[17] Z. Wang, A. C. Bovik, H. R. Sheikh, E. P. Simoncelli, "Image quality assessment: from error visibility to structural similarity", *IEEE T. Image Process.* **13**, 1-13 (2004).

1. Introduction

Computer vision and image processing techniques are found today in all fields of medical science, and are especially relevant to modern ophthalmology. Retinal images are widely used for diagnostic purposes by ophthalmologists. They provide vital information about the health of the sensory part of the visual system. Several diseases that can lead to blindness, such as glaucoma, manifest as anomalies in the retinal image [1]. Automatic segmentation and analysis of retinal images can therefore be used to detect pathological risk or damage, as well as to assist in diagnosis. Such segmentation normally includes the extraction of normal and abnormal features. The normal features of fundus images include the Optic Disc (OD), the fovea and blood vessels (Fig. 1(a)). Exudates and hemorrhages are among the main abnormal features. In the center of the optic disc, Fig. 1(b), one can distinguish a white cup-like area called the Optic Cup (OC).

Glaucoma is a disease characterized by progressive loss of peripheral vision. The decrease of optic nerve fibers caused by ocular hypertension may be visualized in the base of the optic nerve (optic disc). Two commonly used parameters for glaucomatous risk assessment are the cup-to-disc ratio (CDR) and the ISNT rule [2]. The former is estimated as the area occupied by the optic cup within the OD area, whereas the latter is an acronym to indicate the normal distribution of the neuroretinal rim (Inferior ≥ Superior ≥ Nasal ≥ Temporal). The dubbed ISNT rule is widely used in clinical practice. In recent years there has been an increasing interest for semi or automatic determination of the glaucomatous risk as well as the segmentation of the optic nerve head [1]. Li and Chutatape [3] used principal component analysis to locate the OD. Walter *et al* [4] detected the OD by means of morphological filtering techniques and the watershed transformation. In [5,6] they estimate the CDR on a pixel-based segmentation for glaucomatous risk assessment.

In this work we focus on OD segmentation. In the first section we review a previous approach and analyze possible effects in the segmentation of lossy compressed retinal images [7]. In section 3 we introduce a different strategy for OD segmentation based on color mathematical morphology and active contours. We evaluate the results on 20 retinal images and finally outline the conclusions.

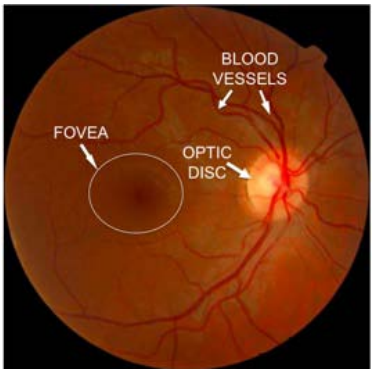

(a)

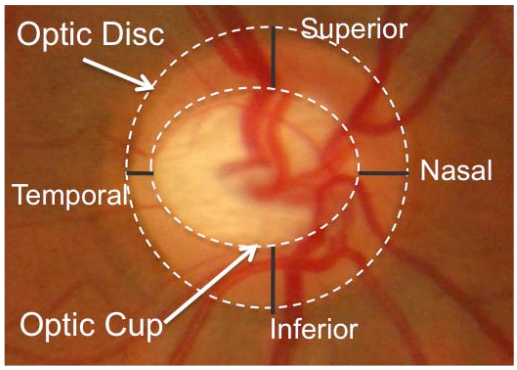

(b)

Fig. 1. (a) Eye fundus image. (b) Optic nerve head region.

2. Optic nerve head segmentation: a previous approach

The OD is one of the main components on fundus images, and its localization is a relevant issue in retinal image analysis. The shape of the OD is an important indicator of various ophthalmic pathologies [1]. Several methods for localizing the OD boundary have been reported in the literature [5,8-10]. In [8] a two-stage method was reported: First, the image was processed using gray-level mathematical morphology to remove the blood vessels. Then a snake was manually placed to detect the OD boundary. The algorithm in [9] uses gradient vector flows to localize the OD. In this section we review an algorithm, previously developed in our research group, for OD feature extraction [5,6]. We analyze its strengths and drawbacks, as well as possible effects in the segmentation of lossy compressed retinal images.

We will briefly describe the main steps of the algorithm developed in [5,6]. The color images of the eye fundus are pre-processed using a sharpening algorithm [11] to smooth noise and sharpen edges by means of the Laplacian of Gaussian operator (LoG). Subsequently, the region of interest (ROI) is manually selected and transformed to polar coordinates for OD boundary extraction. This manual selection is a downside to the algorithm because the user is prompted to assign a manual initial guess for the OD's diameter. In the following stage, the image is transformed to polar coordinates and $\Delta E00$ color differences [12] are calculated between neighbor pixels in all radial directions. Pixels with highest color difference along each radial direction are sought to mark the OD boundary. The algorithm assumes a nearly circular shape as a general hypothesis and seeks on a pixel-based criterion for local distortions of the contour. The OD contour is extracted by interpolation and a back-conversion to Cartesian coordinates. In this approach the algorithm also deals with optic cup extraction by means of color seed selection, thresholding, and boundary extraction in the polar coordinate system. From this double segmentation of both the OD and the OC, they calculate the Cup-to-Disc area ratio and determine whether the ISNT rule is fulfilled.

The resulting segmentation is compared against manually labeled ground-truth produced by an expert. Fig. 2(a) shows a plausible satisfactory segmentation for a circular-shaped OD. There is great similarity as shape is concerned. A drawback of this approach is in the extraction of not so circular-shaped ODs. When the OD tends to a more elliptical shape (which could be a sign of potential risk of glaucoma at early stages) we show that the output may significantly differ from the ground-truth. The segmentation of an elliptical-shaped OD is shown in Fig. 2(b). The arrows indicate regions given by the elliptical shape, which cannot be correctly segmented due to the assumption that the OD is approximately circular.

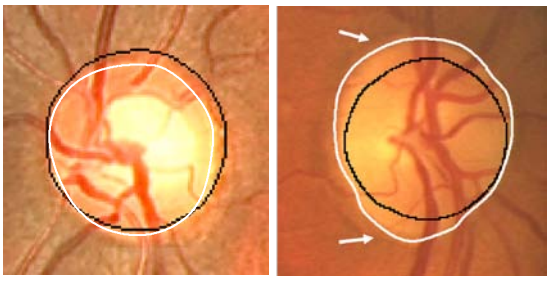

(a) (b)

Fig. 2. Examples for OD segmentation using the algorithm in [5]. Ground-truth in white and contour produced by algorithm in black. (a) nearly circular shaped OD, (b) an elliptical shaped OD.

2.1 Compression effects in segmentation

Nowadays there are many medical instruments that acquire images and, with the purpose of saving memory space, most of these images are saved by default under lossy compression standards, such as classic JPEG. Until recently, the governing premise for lossy compression was that the average human observer would not notice the difference. However, the same cannot be said for computers. So far, standards for a reliable diagnosis have been established in radiology and pathology, whereas in ophthalmology this is still an open issue [15,16]. Therefore, our aim is to identify any compression effects in OD feature extraction, so as to determine possible problems in processing retinal images under compression and establish a safe-ground.

For this analysis we have used the algorithm of [5, 6]. We have used two of the most common lossy compression standards, classic JPEG and JPEG2000, to determine the effect in OD and OC segmentation. A set of 20 color retinal images were compressed for both standards under ratios of 1:2, 1:8, 1:11, 1:22, 1:31 and 1:47. The low compression ratios are used as a reference and the higher ratios correspond to the ones used in a subjective study for the assessment of diabetic retinopathy [15]. Fig. 3(a) shows the segmentation of both OD and OC from the original image without compression in TIFF format. An example of the effects of compression in segmentation of OD and OC is shown in Fig. 3(b)-(g). From these figures we can see that OC segmentation varies considerably under the effects of classic JPEG compression. On the contrary, the OC segmentation under JPEG2000 is more stable. A commonly used parameter to illustrate the corruption in images is the peak signal to noise ratio (PSNR). Although, there exists other parameters that correlate better with perceptual assessment such as the Structural Similarity Index (SSIM) [17], the PSNR gives enough information to set a basis for the comparison of our results. The PSNR was calculated for all compression ratios under JPEG and JPEG2000 standards. In Fig. 4(a) we show the average PSNR for the ROI. The standard JPEG2000 slightly outperforms JPEG.

To appropriately assess the effect in the segmentation we derived a measure based on the l_2-norm of the CDR and ISNT parameters. We recall that I, S, N, and T parameters correspond to the widths of the neuroretinal rim in the inferior,

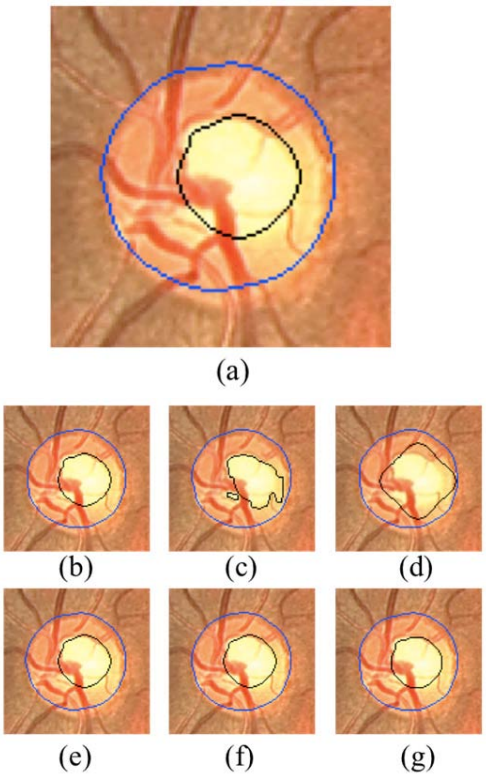

Fig. 3. (a) OD and OC segmentation in image without compression. Segmentation with JPEG compression ratios of (b) 1:2, (c) 1:8, (d) 1:11 and JPEG2000 (e) 1:2, (f) 1:8, and (g) 1:11.

superior, nasal and temporal directions, respectively. In Fig. 1(b), for instance, these quantities correspond to the black segment lengths measured in pixels. For each image, we take a 1-dimmensional vector expressed as $\mathbf{S}^j = \{S_i^j\}$, j=A,B, i=1,…4, $S_1^j = \mathrm{CDR}$, $S_2^j = \mathrm{I}$, $S_3^j = \mathrm{S}$, $S_4^j = \mathrm{N}$; where A and B correspond to the original and the compressed images, respectively. In other words, the elements of each vector correspond to the CDR and I, S, N parameters, where the last three components are normalized to T. Therefore, the normalized distance measure can be calculated as:

$$d = \frac{\left|\mathbf{S}^A - \mathbf{S}^B\right|}{\left|\mathbf{S}^A\right|} = \frac{\sqrt{\sum_{i=1}^{n}\left|S_i^A - S_i^B\right|^2}}{\sqrt{\sum_{i=1}^{n}\left|S_i^A\right|^2}}. \qquad (1)$$

The average distance measure for all 20 images of the set is shown in Fig. 4(b). It can be seen clearly that for very low compression ratios there is a negligible difference, whereas for mid and higher ratios the difference does become significant, particularly for JPEG compression. It is a well

known fact that JPEG and JPEG2000 lossy compression standards introduce random noise given by precision round off, but what might seem to affect a pixel-wise segmentation are the blocking artifacts from classic JPEG. Any algorithm that performs segmentation based on color seed selection is prone to produce inadequate segmentation under high ratio lossy compression. JPEG2000 compression appears to be more reliable than classic JPEG for OD and OC feature extraction.

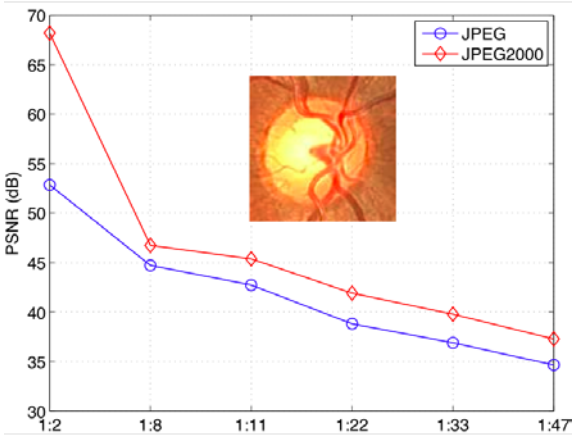

(a)

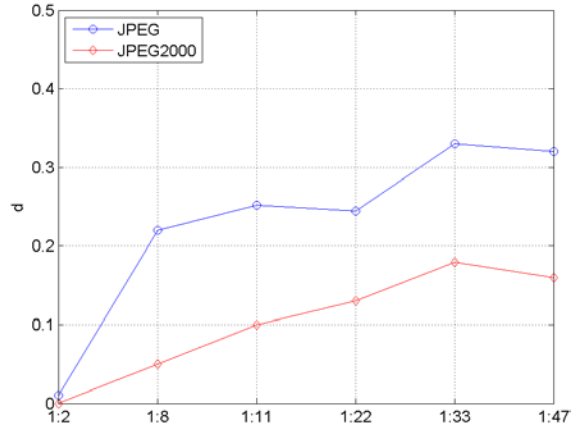

(b)

Fig. 4. (a) PSNR in dB for the different compression ratios under JPEG and JPEG2000 standards. (b) Normalized distance measure for CDR and ISNT.

3. Optic disc localization by means of active contours

In this section we develop a strategy for OD boundary extraction in ocular fundus images. The pre-processing stage consists in performing color mathematical morphology to remove the blood vessel regions. Subsequently, an active contours approach is used to determine the OD boundary. An active contour is an energy-minimizing spline guided by external constraint forces influenced by image forces that pull it toward features such as lines and edges [14]. Mendels *et al* [8] presented a technique to localize the OD based on active contours formulated on gray-level images. In this work we formulate our approach in the Lab color space to take full advantage of the color features available for the pre-processing and feature extraction stages.

The segmentation algorithm is fully automatic. We have processed 20 color 24 bit-depth RGB fundus images of size 768 × 576 pixels. All images were acquired using a Topcon TRC-NW6S retinograph and a 3CCD Sony DXC-990P camera. The accuracy of the method is compared to ground-truth manual segmentation produced by an expert. The manual segmentation was carried out by an ophthalmologist with the use of an assisted graphical user interface developed in our research group.

3.1 Color mathematical morphology

Active contour methods generally work by locking onto homogeneous regions of a given image. This task is made extremely difficult since the OD region is fragmented into multiple subregions by blood vessels. Furthermore, the blood vessels enter the OD from different directions with a general tendency to concentrate around the nasal side of the OD region. Mathematical morphology can extract important shape characteristics and also remove irrelevant information. It typically probes an image with a small shape or template known as a structuring element. Using gray-level morphology, the operation can be applied to the intensity or lightness channel. Osareh *et al* [9] showed that in retinal images color morphology outperforms gray-level morphology, which results in more homogeneous regions and better preservation of the OD edges. They used a definition of color morphology within the CIELAB [12] color space (from now on Lab space) based on a color difference metric. We performed a closing operation, i.e. dilation to first remove the blood vessels and then an erosion to approximately restore the boundaries to their former position.

In color morphology, each pixel must be considered as a vector of color components.

Definitions of maximum and minimum operations on ordered vectors are necessary to perform basic operations. Hence, for each arbitrary point x in the color space, the definitions for dilation (I_d) and erosion (I_e) by structuring element B are:

$$I_d(x) = \{I(y) : I(y) = \max[I(z)], z \in B_x\}, \quad (2)$$

$$I_e(x) = \{I(y) : I(y) = \min[I(z)], z \in B_x\}. \quad (3)$$

Osareh et al. [9] introduced a lexicographical order to color morphology in the Lab space such that basic morphological operations could be performed. This is a problem-oriented formulation based on the knowledge that the OD region contains contrasting pixels: bright, almost saturated regions crossed by dark blood vessel regions. These color differences will reside in well-separated regions of the Lab color space. Given that color differences in the Lab space correspond to the metric distance between them, the basic morphological operations of dilation and erosion can be defined using the color difference of all pixels within the structuring mask to a certain reference point. The color difference within the Lab color space can be obtained using the Euclidean norm, and the reference point is established at the origin (0, 0, 0). The dilation is the furthest point from the origin, and the erosion is the point closest to the origin. The closing operation involves a dilation followed by an erosion. An example of closing using this formulation with a disc type-structuring element is shown in Fig. 5(a)-(b). It is evident that this approach produces a more homogeneous region while approximately preserving the OD edges Fig. 5(c).

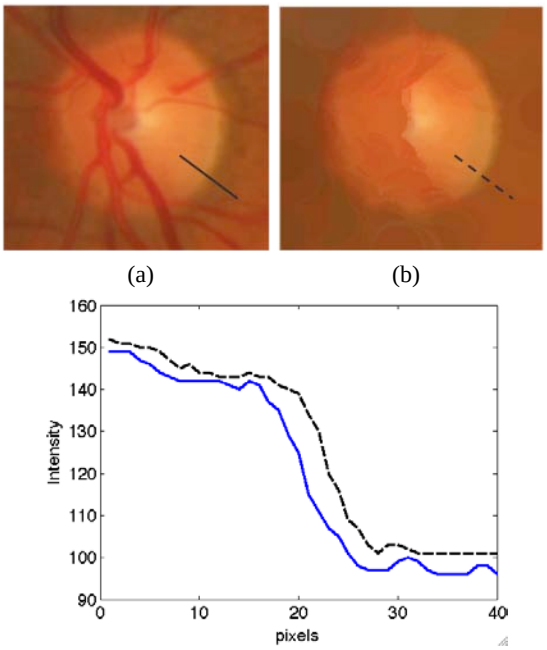

Fig. 5. Color morphology closing. (a) Original ROI (150x150 pixels) with OD inside. (b) Lab closing with a 25x25 disc-type structuring element. (c) Intensity profile cuts from (a) solid and (b) dashed.

3.2 Optic disc boundary extraction

The OD boundary is determined by fitting a geometric active contour model, namely the Chan-Vese [14] model. The performance of the methodology is evaluated by fitting the active contour onto the OD and comparing the resulting region against hand-labeled ground truth information. In general the active contour consists of a set of points placed near the contour of interest, which are gradually brought closer to the exact shape of the desired region in the image. This is carried out through iterative minimization of an energy function. The Chan-Vese model [14] establishes the following energy function for an image u_0:

$$F(c_1, c_2, C) = \int_{outside(C)} |u_0(x,y) - c_1|^2 dx dy + \int_{inside(C)} |u_0(x,y) - c_2|^2 dx dy + g(C), \quad (4)$$

where C is a piecewise parameterized curve (contour), g is any function evaluated at C, and c_1 and c_2 represent the average intensity value of u_0 inside and outside the curve, respectively. Minimizing the fitting error in (4), the model looks for the best partition of u_0 taking only two values, namely c_1 and c_2, and with one edge C, the boundary between these two regions, given by $\{u_0 \approx c_1\}$ and $\{u_0 \approx c_2\}$. Now, let us define a signed distance function ϕ that is zero exactly at C, that increases in absolute value with respect to the distance from C and that is positive inside and negative outside, as shown in Fig. 6. By doing so, we have defined implicitly the curve as, $C = \{(x, y) \mid \phi(x, y) = 0\}$. Therefore, the energy function can be expressed as:

$$F(c_1, c_2, \phi) = \int_{\phi>0} (u_0(x,y) - c_1)^2 H(\phi) dx dy + \int_{\phi<0} (u_0(x,y) - c_2)^2 (1 - H(\phi)) dx dy, \quad (5)$$

where $H(.)$ is the Heaviside function. Keeping c_1 and c_2 fixed, and minimizing F with respect to ϕ we obtain the associated Euler-Lagrange equation for ϕ. Parameterizing the descent direction by an artificial time $t \geq 0$ (or number of iterations), the equation in $\phi(t,x,y)$ (with $\phi(0,x,y) = \phi_0(x,y)$ defining the initial contour) is:

$$\frac{\partial \phi}{\partial t} = \delta(\phi)\left[div\left(\frac{\nabla \phi}{|\nabla \phi|}\right) - (u_0 - c_1)^2 - (u_0 - c_2)^2 \right]. \quad (6)$$

where $\delta(.)$ is the Dirac function. This partial differential equation can be solved numerically using a finite difference scheme. In relation to the problem at hand, we take the initial contour to be a circle big enough to fully contain the OD. From this circle a signed distance map is built for ϕ_0, fulfilling the condition to be positive inside the contour, zero exactly at the boundary, and negative outside. The iterative process consists in calculating the force from the image information, from the curvature penalty, and later evolving the curve (i.e. calculating ϕ_{n+1}).

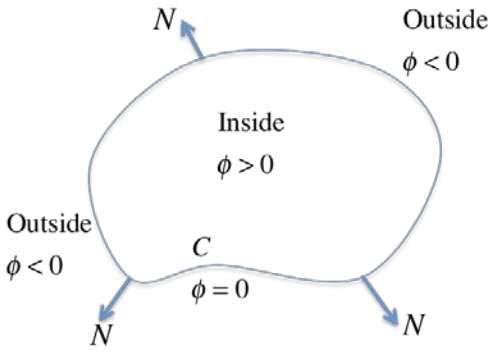

Fig.6. Curve *C* propagating in the normal direction.

3.3 Results

The ROI is selected manually as a window of 150×150 pixels, with the whole OD inside Fig. 5(a). We applied the Lab closing to all images using a symmetrical 25×25 pixels disc-structuring element since the blood vessels were determined not to be wider than 20 pixels. The Lab closing allowed to remove the blood vessels cleanly and provided the required uniform OD region Fig. 5(b) to initialize the active contour. The active contours approach requires an intensity or gray-scale image to perform the optimization procedure. Therefore, instead of solely using the lightness channel *L* and, more importantly, to be consistent with the color mathematical morphology approach, we decided to use the weighting function based on the Euclidean distance within the Lab space. This feature is fundamental to obtain a uniform OD region because our approach is based on the segmentation of pixels with similar color properties.

Following the color morphological pre-processing step, we initialized the contour as a circle with the center at the brightest area and with a diameter equivalent to 80% of the ROI diameter. From these initial conditions the active contour iteratively shrank towards the final boundary. The number of iterations for the final contour convergence was determined empirically and set to 450 for all cases. In Fig. 7(a)-(c) we show the hand-labeled ground-truth OD, the initial contour, and the final contour respectively.

In Fig. 7(d) we show the hand-labeled boundary together with the final contour to illustrate the close match achieved. We quantify the accuracy of the boundary localization against the manually labeled ground-truth produced by an expert. We use a simple and effective overlap measure of the match between two regions as:

$$M = \frac{n(R \cap T)}{n(R \cup T)} \times 100\,, \quad (7)$$

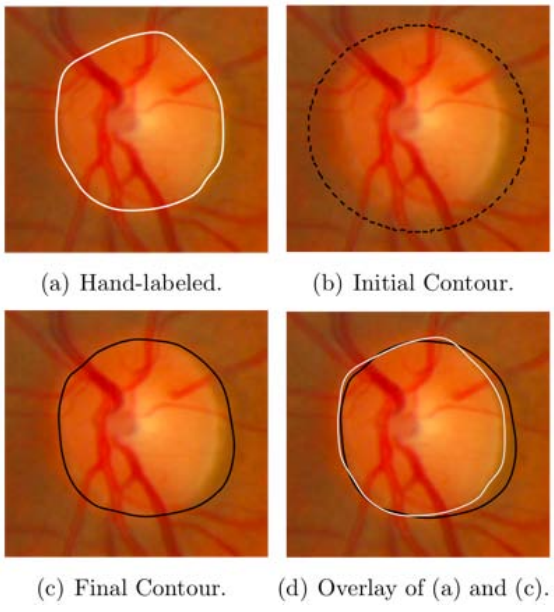

Fig.7. Optic disc boundary extraction results.

where R and T correspond to the ground-truth and the final OD contour region respectively, and $n(.)$ is the number of pixels in a region. In the optimal case, when both contours perfectly match $M = 100$. The measure M represents the accuracy. When compared with the hand-labeled ground-truth information from the expert, our method was able to localize the OD pixels in all test images with an average accuracy of 85.67 % ($\sigma = 7.82$). Additional tests are shown in Fig. 8 for some ODs whose shapes differ significantly from a circle. Notice the excellent agreement in Fig. 8(b) and the improvement achieved in Fig. 8(c) in comparison with the previous segmentation of Fig. 2(b).

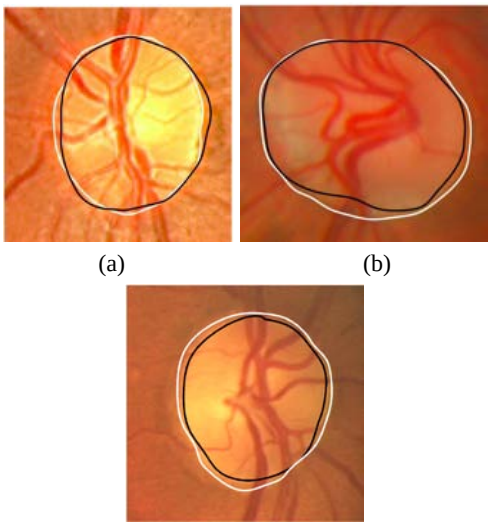

(a) (b)

(c)

Fig.8. Other OD segmentation results. Ground-truth in white and algorithm output in black. M values are: (a) 92.61, (b) 90.32, (c) 88.15.

4. Summary and conclusions

In this work we have discussed two different approaches towards OD segmentation. The analysis of the algorithm in [5,6] revealed the need for a more general and robust approach, which would enable the segmentation of OD boundaries that differ considerably from a circular shape. As regards to compression effects in segmentation of the optic nerve head, we determined that degradation introduced by lossy compression plays an important role and cannot be neglected when processing compressed images. Nonetheless, our results showed that JPEG2000 compression might provide a safer ground for retinal image segmentation than classical JPEG. A different strategy for OD localization based on active contours was developed. The pre-processing stage consisted in performing color mathematical morphology. This provided a vessel-free OD region with uniform color distribution and preservation of sharp edge position. The active contours algorithm for OD segmentation yielded a fair approximation to the actual hand-labeled OD. Our method was able to achieve an average accuracy rate in pixel classification of 85.67 % ($\sigma = 7.82$).

Acknowledgements

The authors thank Isabel Martínez (MSc in Optometry) for helpful discussions and for providing some of the retinal images analyzed in the paper. This research has been funded by the Spanish Ministerio de Ciencia e Innovación y Fondos FEDER (project DPI2009-08879). The first author also thanks the Spanish Ministerio de Educación for an FPU doctoral scholarship.

